



# Field Quality Measurements of Fermilab Nb<sub>3</sub>Sn Common Coil Dipole Model

V. S. KASHIKHIN, N. ANDREEV, J. DIMARCO, S. FEHER, V. V. KASHIKHIN,  
M. LAMM, I. NOVITSKI, D. ORRIS, P. SCHLABACH, C. SYLVESTER,  
M. TARTAGLIA, G. VELEV, A. V. ZLOBIN

**Abstract**--A short model of single-layer Nb<sub>3</sub>Sn common coil magnet has been fabricated and is being tested at Fermilab. This paper summarizes results of magnetic measurements in this model. The geometrical harmonics, coil magnetization and iron saturation effects, ramp-rate dependence, field decay and the "snap-back" effect at injection are presented.

**Index Terms**--Superconducting accelerator magnet, magnetic field measurements, magnetization, eddy currents.

## I. INTRODUCTION

HIGH field accelerator magnets based on shell and common coil configurations [1]-[2] are being developed at Fermilab for future hadron colliders. These magnets are designed for a nominal field of 10-12 T in a magnet bore of 40-50 mm. New high-performance Nb<sub>3</sub>Sn superconductor is used in order to achieve the design fields at nominal operation temperature of 4.5 K. The first 1-m long common coil dipole model HFDC01 was recently fabricated and is being tested at the Fermilab Vertical Magnet Test Facility. During testing, the magnetic measurements were taken at 4.5 K in two apertures. The measurements were made at excitation currents up to 12 kA due to restrictions imposed by the magnet quench current reached at present time.

## II. MAGNET DESIGN

Magnetic design and parameters of the HFDC01 short model and details of the magnet technology and model fabrication are reported elsewhere [3]-[4]. The baseline design consists of a single-layer common coil with a 40 mm bore and cold iron yoke. Fig. 1 shows both a 3D view of the magnet and the picture of the lead end of the magnet cold mass.

The coils were wound from the reacted rectangular Rutherford-type cable made of 59 Nb<sub>3</sub>Sn strands, each 0.7 mm in diameter. The strands were manufactured by OST using the Modified Jelly Roll (MJR) process. A 0.16 mm thick pre-preg fiberglass tape and 0.08 mm Kapton tape were co-wound with the cable during coil winding as the inter-cable insulation.

The critical current for the virgin and extracted from the

cable strands reacted with cable as witness samples measured at 12 T and 4.2 K and was in the range of 371-417 A. The magnet quench current based on the short sample limit of the witness samples and assuming 6 % bending degradation was 23.3 kA. Measured strand and cable RRR varied from 4 to 35.

Each racetrack coil consisted of 56 turns wound from the reacted cable. Due to larger conductor size after reaction, the as-built geometry had to contain two turns less per racetrack coil with respect to the baseline, 58-turns design. One turn was symmetrically removed from each pole block in order to minimize distortions of the field quality.

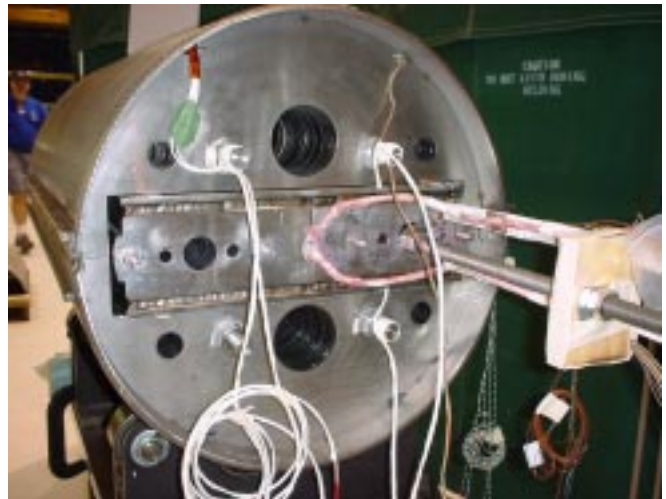
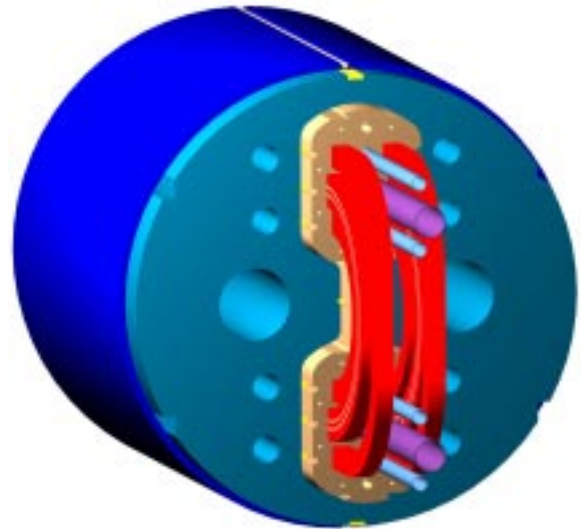


Fig. 1. Model 3D view and assembled cold mass.

Manuscript received October 20, 2003. This work was supported by the U.S. Department of Energy.

Authors are with the Fermi National Accelerator Laboratory, P.O. Box 500, Fermilab, Batavia, IL 60510, USA (email: kash@fnal.gov).

The support structure of the model consisted of stainless steel collars, which provided precise block positioning and stress management. Collared coil was surrounded by the vertically split 0.4 m long iron yoke and 10-mm thick stainless steel skin. The cold-mass had outer diameter of 580 mm and length of ~1 m. Two 50-mm end plates restricted longitudinal motion of coil ends under Lorentz force.

### III. MEASUREMENT SYSTEM

A vertical drive rotating coil system was used for magnetic measurements. The coil used has a nominal diameter of 2.5 cm and length 25 cm. A tangential winding measured the field harmonics; dipole windings measured the main field and allowed bucking of the large dipole component in the tangential winding signal. Coil winding voltages as well as magnet current were read by HP3458 DVMs triggered simultaneously by an angular encoder on the probe shaft to synchronize measurements of the field and current. A centering correction was performed using feed down of higher order allowed harmonics to lower order unallowed harmonics (18, 22 pole to 16, 20 pole).

The field in the magnet body was represented in terms of harmonic coefficients defined by the power series expansion:

$$B_y + iB_x = B_1 \times 10^{-4} \sum_{n=1}^{\infty} (b_n + ia_n) \left( \frac{x + iy}{r_0} \right)^{n-1},$$

where  $B_x$  and  $B_y$  are horizontal and vertical transverse field components,  $B_1$  is the dipole field strength, and  $b_n$  and  $a_n$  are the  $2n$ -pole coefficients ( $b_1=10^4$ ) at a reference radius  $r_0$ .

A Cartesian coordinate system was defined with the  $Z$ -axis at the center of the magnet aperture, pointing from return to lead end, the  $X$ -axis horizontal and pointing to the right of an observer who faces the magnet from the lead end, and the  $Y$ -axis pointing upwards. In this paper field harmonics are presented at the reference radius of 10 mm, and  $Z = 0$  mm corresponds to the coil center.

### IV. MEASUREMENT RESULTS

The model was tested in boiling liquid helium at 4.5 K. The maximum current achieved was ~13.7 kA, which is ~60% of the expected magnet short sample limit [4]. Magnetic measurements were performed in both apertures in two consequent thermal cycles. The aperture closest to the leads is called in this paper as ‘‘aperture I’’ whereas the other one is called as ‘‘aperture II’’.

#### A. Geometrical Harmonics

To evaluate harmonics distribution along the magnet, the probe was consequently centered at  $Z=-750, -500, -250, 0, 250, 500, 750$  mm after the ramp up to 5 kA, then up to 12 kA and back to 5 kA. The geometrical harmonics were determined as average values between up and down ramps at 5 kA for every  $Z$ -position. The comparison of measured and calculated in 3D case for the as-built geometry harmonics is presented in Tables I-III. In order to be comparable with the measurements,

harmonics calculated in 3D case were integrated over the probe length of 250 mm centered at the same  $Z$ -positions. To represent the end fields, the calculated and measured harmonics were integrated for the probe centered at the following  $Z=-750, -500$  and  $-250$  mm for the return end and at  $Z=250, 500$  and  $750$  mm for the lead end and normalized to the magnetic lengths of the relevant ends.

One can see an excellent (for  $Nb_3Sn$  magnet) correlation between the calculated and measured harmonics in the magnet body. The integrated harmonics in the magnet return end are also consistent with the calculations. These results confirm efficiency of the coil support structure for maintaining the nominal coil geometry and thus the field quality during magnet assembly and operation. Field calculations in the magnet lead end were not done up to date, but are foreseen in the future.

TABLE I  
GEOMETRICAL HARMONICS IN MAGNET BODY

n	Calculated ‘‘as built’’ values		Measured in aperture I		Measured in aperture II	
	$a_n$	$b_n$	$a_n$	$b_n$	$a_n$	$b_n$
2	-3.298	-	-3.28	0.16	-3.57	-1.26
3	-	10.638	0.23	10.30	-0.20	10.37
4	0.034	-	-0.35	0.02	-0.66	-0.17
5	-	0.353	0.04	0.73	-0.04	0.79
6	-0.040	-	0.00	-0.01	0.01	0.01
7	-	-0.083	0.00	-0.06	-0.00	-0.05
8	-0.003	-	used for the centering correction			
9	-	-0.008	-0.00	-0.03	-0.00	-0.03

TABLE II  
INTEGRATED GEOMETRICAL HARMONICS IN MAGNET RETURN END

n	Calculated ‘‘as built’’ values		Measured in aperture I		Measured in aperture II	
	$a_n$	$b_n$	$a_n$	$b_n$	$a_n$	$b_n$
2	9.164	-	9.22	5.26	3.55	-7.52
3	-	6.657	-0.27	9.80	1.01	9.35
4	1.866	-	1.18	-0.06	0.98	-0.22
5	-	-0.068	0.04	0.07	-0.02	-0.05
6	0.158	-	0.24	0.01	0.27	-0.01
7	-	-0.005	-0.01	0.03	0.01	0.06
8	-0.006	-	used for the centering correction			
9	-	-0.006	-0.00	-0.02	-0.00	-0.02

TABLE III  
INTEGRATED GEOMETRICAL HARMONICS IN MAGNET LEAD END

n	Measured in aperture I		Measured in aperture II	
	$a_n$	$b_n$	$a_n$	$b_n$
2	-17.03	-3.04	2.95	10.35
3	-0.18	-2.38	2.45	4.46
4	3.27	-0.10	2.75	-0.46
5	-0.12	0.06	0.05	-0.06
6	0.25	-0.03	0.28	0.02
7	-0.00	0.05	-0.00	0.03
8	used for the centering correction			
9	0.00	-0.01	-0.00	-0.02

### B. Iron Saturation

The transfer function and skew quadrupole measured in 0-12-0 kA current cycle in the magnet body and calculated in both 2D and 3D cases are shown in Figs. 2-3. The calculated in 3D case values were integrated over 250 mm region, centered at  $Z=0$  mm. One can see the iron saturation effect in both plots for the fields above 2.5 T. This effect leads to a deviation of the transfer function by 3.5% and skew quadrupole by 13 units at 5 T with respect to the 2D values. The calculated 3D values match the measurements well for the fields above 1.5 T. Deviations at lower fields are presumably caused by the magnetization of the stainless steel collar.

A comparison of the 2D and 3D calculations with the magnetic measurements suggests that the magnet model is too short and requires 3D magnetic analysis. Although the high field level was not achieved yet during the magnet tests, the good correlation of measurements with the 3D calculations proves that the iron saturation effect can be accurately predicted and optimized in numerical simulations for this type of magnet.

### C. Coil Magnetization

The effect of coil magnetization on the normal sextupole measured and calculated in the magnet body is shown in Fig. 4 (the geometrical components reported in Table I were subtracted from the presented data). The up-ramp branches of both measured and calculated curves match well at the fields above 2 T. The discrepancy in the down-ramp branches at higher fields is due to superconductor re-magnetization effect not included in the calculation model.

One can clearly see the iron saturation effect in both loops, which would otherwise be symmetric with respect to the horizontal axis. Due to peculiarities of magnetization flux distribution in the single-layer coil design [6] the calculated and measured widths of the loops in Fig. 4 is a factor of 5 smaller than in the cos-theta  $Nb_3Sn$  dipole models tested earlier [5] in spite of larger coil cross-section area in the common coil magnet.

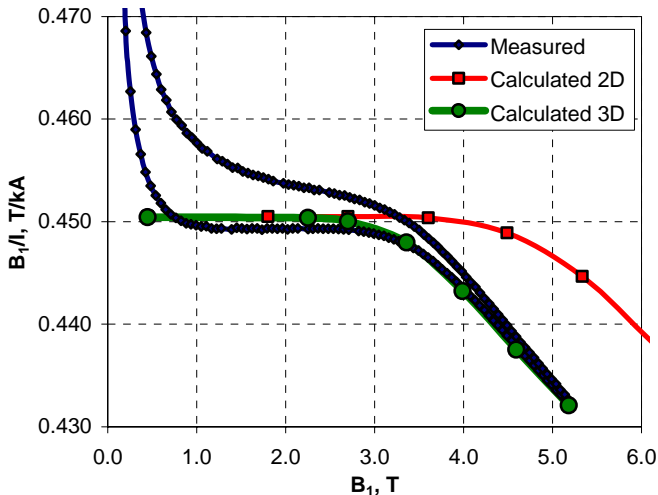


Fig. 2. Transfer function in the magnet body.

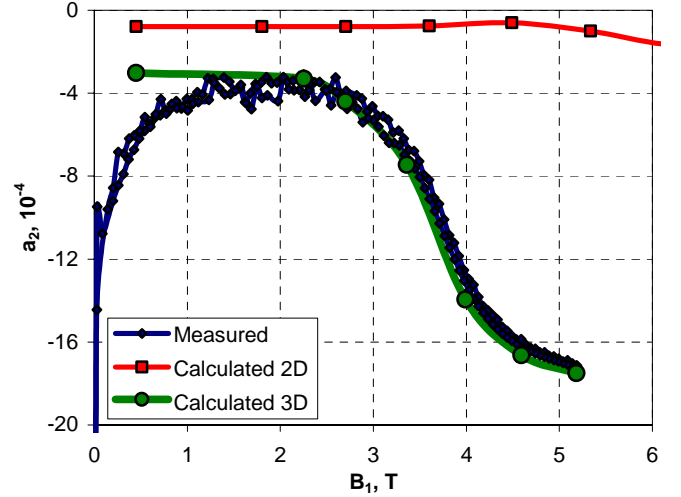


Fig. 3. Skew quadrupole in the magnet body.

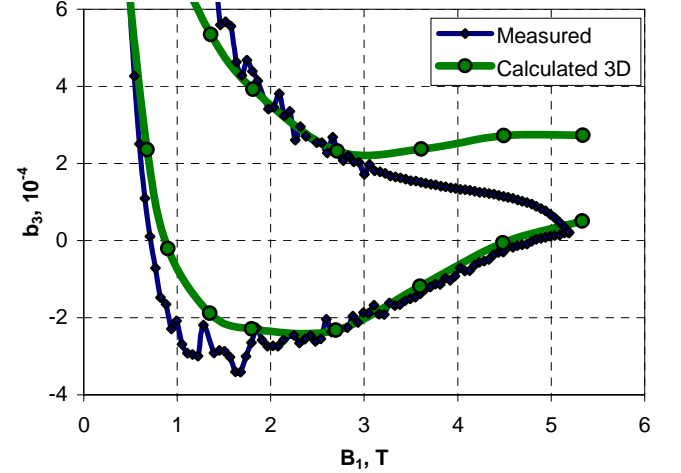


Fig. 4. Sextupole hysteresis in 0-12-0 kA cycle.

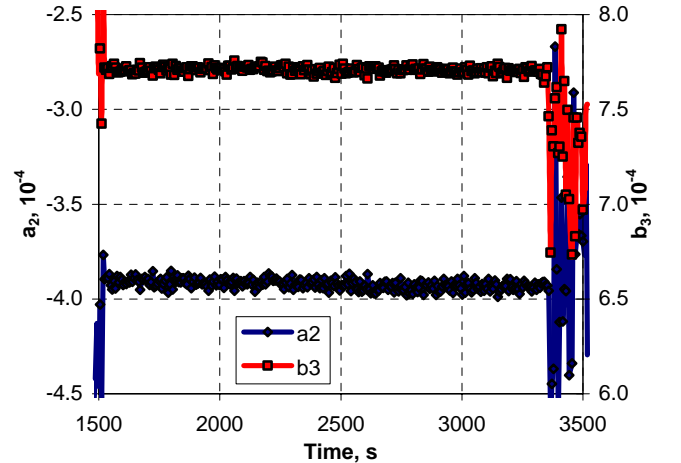


Fig. 5. Skew quadrupole and sextupole at 2.4 kA plateau.

### D. Harmonics Decay and "Snapback"

To check for dynamic effects at injection-like conditions, the field measurements were performed at the current plateau of 2.4 kA during 30 minutes, following conditioning pre-cycle up to 12 kA. Measured time dependences of the skew

quadrupole and sextupole at the plateau are presented in Fig. 5. Changes in harmonics during this period of time were very small (less than 0.3 units) with respect to those observed in most of NbTi accelerator magnets. This result is consistent with similar measurements of dynamic effects in cos-theta Nb<sub>3</sub>Sn dipole models [7].

### E. Eddy Currents

The harmonic ramp-rate dependence was measured in three consequent current cycles up to 12 kA with the current ramp rates of 20 A/s, 40 A/s and 80 A/s. Fig. 6 shows the measured sextupole loops. It can be seen that the dependence of the sextupole on the current ramp rate is very small, which is also the case for all other harmonics. Absence of the eddy currents in the cable is related to the high interstrand resistance, presumably created during the cable reaction with synthetic oil under no transverse pressure [8]. This result is consistent with the AC losses measured in this model and presented in Fig. 7.

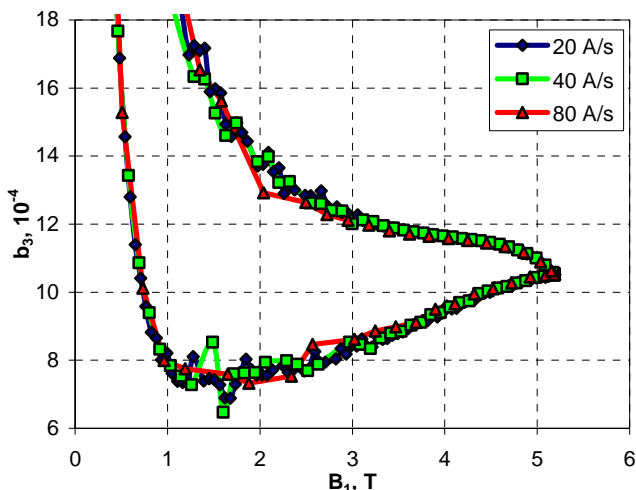


Fig. 6. Measured sextupole hysteresis at different current ramp rates.

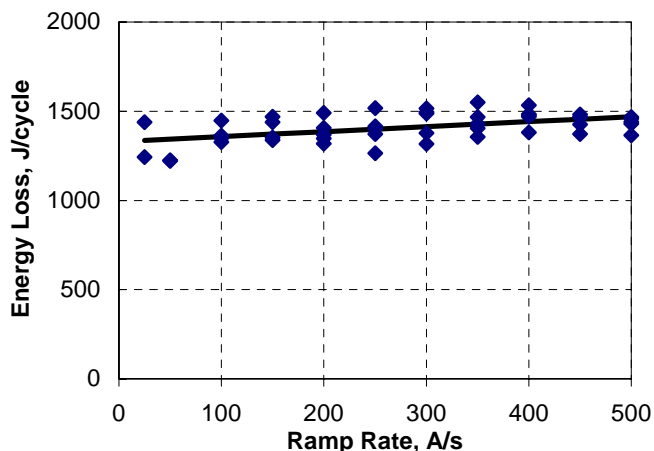


Fig. 7. AC losses in the current cycle 500-6500-500 A at different current ramp rates.

## V. CONCLUSION

Magnetic field measurements were performed in the first Fermilab common coil dipole model. Due to the limited

quench performance, the maximum current during magnetic measurements was limited by 12 kA. In spite of this restriction, it was possible to evaluate most interesting effects, including iron saturation.

Field quality measurements are consistent with the 3D magnetic analysis based on the as-built coil geometry, which confirms the high efficiency of the designed mechanical support structure for maintaining of the proper coil geometry and thus the field quality.

Low coil magnetization effect is consistent with the predictions for this magnet design. No special field correction is required for this magnet even for high-Jc superconductor with large effective filament size.

Measured field decay and “snap-back” effects are small. Virtual absence of the dynamic effects in the field quality, observed in this model and in few previously tested Nb<sub>3</sub>Sn shell-type dipole magnets is an exciting result that may essentially simplify a field correction system and operation of future hadron colliders utilizing high field Nb<sub>3</sub>Sn magnets.

## REFERENCES

- [1] G. Ambrosio, N. Andreev, E. Barzi, D. Chichili, V.V. Kashikhin, I. Terechkine, S. Yadav, R. Yamada, A.V. Zlobin, “Development of cos-theta Nb<sub>3</sub>Sn dipole magnets for VLHC”, Proceedings of the 2001 Particle Accelerator Conference, Chicago, Illinois, pp.3427-3429.
- [2] G. Ambrosio, N. Andreev, E. Barzi, P. Bauer, D. Chichili, K. Ewald, L. Imbasciati, V.V. Kashikhin, P. Limon, I. Novitski, J-M. Rey, R. Scanlan, S. Yadav, R. Yamada, A.V. Zlobin, “Design and development of Nb<sub>3</sub>Sn single-layer common coil dipole magnet for VLHC”, Proceedings of the 2001 Particle Accelerator Conference, Chicago, Illinois, pp.3409-3411.
- [3] G. Ambrosio, N. Andreev, E. Barzi, P. Bauer, D.R. Chichili, K. Ewald, S. Feher, L. Imbasciati, V.V. Kashikhin, P.J. Limon, L. Litvinenko, I. Novitski, J.M. Rey, R.M. Scanlan, S. Yadav, R. Yamada, A.V. Zlobin, “R&D for a single-layer Nb<sub>3</sub>Sn common coil dipole using the react-and-wind fabrication technique”, MT-17, IEEE Transactions on Applied Superconductivity, Vol. 12, No. 1, March 2002, pp.39-42.
- [4] V.S. Kashikhin et al., “Development and test of common coil dipole with Nb<sub>3</sub>Sn reacted cable”, This conference.
- [5] E. Barzi, D. Chichili, J. DiMarco, V.V. Kashikhin, M. Lamm, P. Schlabach, A.V. Zlobin, “Passive correction of the persistent current effect in Nb<sub>3</sub>Sn accelerator magnets”, ASC2002, IEEE Transactions on Applied Superconductivity, Vol. 13, No. 2, June 2003, pp.1270-1273.
- [6] V.V. Kashikhin, A.V. Zlobin, “Correction of the persistent current effect in Nb<sub>3</sub>Sn dipole magnets”, ASC2000, IEEE Transactions on Applied Superconductivity, Vol. 11, No. 1, March 2001, pp.2058-2061.
- [7] E. Barzi, R. Carcagno, D. Chichili, J. DiMarco, H. G. Glass, V.V. Kashikhin, M. Lamm, J. Nogiec, D. Orris, T. Peterson, R. Rabehl, P. Schlabach, C. Sylvester, M. Tartaglia, J.C. Tompkins, G. Velez, A.V. Zlobin, “Field Quality of the Fermilab Nb<sub>3</sub>Sn Cos-theta Dipole Models”, paper MOPLE020, EPAC2002, Paris, June 3-7 2002, p.2403.
- [8] G. Ambrosio, E. Barzi, D. Chichili, L. Elementi, A.V. Zlobin, “Measurement of Inter-Strand Contact Resistance in Epoxy Impregnated Nb<sub>3</sub>Sn Rutherford Cables”, CEC/ICMC 2003, Anchorage, Alaska, September 22-25, 2003.